Temperature-driven magnetic and structural transitions in multiferroic Lu(1-)Sc FeO3

Andrius Pakalniškis, Gediminas Niaura, Rimantas Ramanauskas, Dmitry Karpinsky, Guillaume Rogez, Marc Lenertz, Jerome Robert, Pierre Rabu, Shih-Wen Chen, Thomas Chung-Kuang Yang, et al.

Temperature-Driven Magnetic and Structural Transitions in Multiferroic $Lu_{(1-x)}Sc_xFeO_3$

Andrius Pakalniškis[1,*], Gediminas Niaura[2], Rimantas Ramanauskas[2], Dmitry Karpinsky[3], Guillaume Rogez[4], Marc Lenertz[4], Jerome Robert[4], Pierre Rabu[4], Shih-Wen Chen[5], Thomas Chung-Kuang Yang[6,7], Ramūnas Skaudžius[1], Aivaras Kareiva[1]

[1] Institute of Chemistry, Vilnius University, Naugarduko 24, LT-03225 Vilnius, Lithuania
[2] Center for Physical Sciences and Technology (FTMC), Sauletekio Ave. 3, LT-10257, Vilnius, Lithuania
[3]Namangan Engineering-Construction Institute, Islam Karimov Street 12, Namangan UZ-160103, Uzbekistan
[4]Institut de Physique et Chimie des Matériaux de Strasbourg (UMR 7504 CNRS-Université de Strasbourg), Strasbourg, France
[5]Graduate Institute of Automation Technology, National Taipei University of Technology, Taipei Taiwan
[6]Precision Analysis and Materials Research Center, National Taipei University of Technology, Taipei, Taiwan
[7]Department of Chemical Engineering and Biotechnology, National Taipei University of Technology, Taipei Taiwan

Abstract: Novel metastable hexagonal $Lu_{(1-x)}S_xFeO_3$ compounds were prepared by an ethylene glycol-based small molecule sol-gel synthesis route. Samples were investigated by means of XRD, Raman spectroscopy, XPS, SEM and magnetometry techniques. Based on the obtained data several different phase composition regions were discovered at room temperature depending on the Sc content. Three dominant phases were observed and denoted as the orthorhombic *Pnma*, hexagonal *P6₃cm*, and cubic *Ia-3* with the hexagonal phase being stable without any additional phases when $0.40 \leq x < 0.65$. Temperature dependent structural analysis allowed for the construction of the phase diagram which revealed that upon increasing Sc content the reversible polar to non-polar phase transition temperature can be decreased from above 1200 °C (when x = 0.15) to around 800 °C (x = 0.75). SEM analysis indicated a rapid reduction in particle size from ~2.726 μm when x = 0 down to ~0.962 μm when x = 0.75, however in the case when x = 1, an increase in particle size was observed. XPS analysis confirmed the elemental composition and its changes as well as the stability of the 3+ oxidation state of the iron ions. Magnetization measurements confirmed a non-zero room temperature magnetization as well as the spin reorientation transitions whose critical temperatures T_N increases from 156 K (x = 0.25) to 170 K (x = 0.75).

Keywords: multiferroics, sol-gel processing, magnetic transitions, structural properties

*Corresponding author: E-mail: andrius.pakalniskis@chgf.vu.lt

1. Introduction

Complex oxides based on transition metal elements constitute a class of materials that possess a broad spectrum of different properties depending on the chemical composition and crystal structure. The different phenomena include luminescence, ferromagnetism, ferroelectric properties, etc. [1–4]. One particular group of oxides has attracted a large amount of interest from scientists and is referred to as Perovskite compounds [5–8]. The abundant interest in perovskites arises mostly due to a particular variability of the symmetry of the crystal structure they possess. The ideal perovskite lattice is a cubic one with a *Pm-3m* (# 221) space group with a nominal formula of ABO_3 [9]. By varying the elemental composition in A- and B- positions, the cubic crystal structure can be significantly distorted, thus changing the symmetry [8,10]. This allows perovskites to possess a lot of the aforementioned properties. In some rare cases, perovskites can exhibit even multiferroicity [11,12]. Multiferroicity refers to the combination of at least two primary ferroic orders in a single system. The most desirable combination is the one of ferroelectric and ferromagnetic properties as it would allow for many novel applications such as low power electronic memory, spintronic devices, sensors, etc. [12–14].

The applications of single phase multiferroic compounds sound extremely promising, however, several difficult hurdles need to be overcome beforehand. The initial challenge arises from the conflicting nature of the traditionally known origins of ferroelectricity and ferromagnetism. For a compound to be ferroelectric the empty 3d orbitals are needed for hybridization (this is referred to as ferroelectricity of displacive-type), while for a compound to be strongly ferromagnetic unpaired electrons in the same orbitals are needed [15]. As of now, several different ferroelectricity causing effects have been discovered: the lone-pair mechanism in which ferroelectricity is caused by the non-hybridized electrons in 6s orbital, the geometric

ferroelectricity mechanism in which ferroelectricity is caused by the space filling and geometric constraints which displace the atoms in the lattice [16,17], as well as the charge ordering and spin driven mechanisms [18,19]. The second challenge is that the magnetoelectric coupling, the interaction between magnetic and electrical ordering, is often relatively weak. This problem arises mainly in multiferroic compounds where magnetic and electric orders occur independently of each other, such compounds are referred to as Type I. Type II multiferroic compounds possess magnetic and electrical orders that emerge jointly, however, this phenomenon is usually observed only for spin driven ferroelectricity, that produces relatively low polarization values [20]. The third challenge is that it is quite difficult to obtain both magnetic and electric orders at or above room temperature, required for practical applications. As such, a lot of fundamental, practical, and theoretical investigations are still needed [21].

Due to the aforementioned reasons the amount of room temperature single phase multiferroic compounds is quite scarce [22]. The most well-known multiferroic $BiFeO_3$ is a rhombohedral perovskite with the crystal structure described by the space group *R3c* (#161) [23]. Bismuth ferrite combines lone pair driven ferroelectricity with an antiferromagnetic order caused by the cycloidal arrangement of the magnetic moments of Fe ions forming magnetic sublattice [24]. This provides a quite high polarization with Tc ~ 1100 K and a Néel temperature of T_N ~ 640 K [5,25]. However bismuth ferrite suffers from several significant drawbacks, mainly that it is difficult to synthesize, due to the volatility of bismuth and a formation of competing impurity phases, large leakage currents and the presence of antiferromagnetic order instead of a ferromagnetic one limiting its practical applications [26]. One other possible room temperature multiferroic compound that has attracted a lot of attention recently is the hexagonal variant of $LuFeO_3$ (h-$LuFeO_3$) [27,28]. Under normal conditions, $LuFeO_3$ possesses a distorted perovskite

structure with orthorhombic symmetry. It is weakly ferromagnetic and non-polar thus it could hardly be described as multiferroic [29,30]. However, when the hexagonal structure with the space group *P6$_3$cm* (#185) is stabilized, ferroelectricity is obtained due to the geometric factors displacing a part of the Lu atoms in the lattice. This displacement is produced during the transition from high temperature paraelectric phase (space group *P6$_3$/mmc*) to the room temperature ferroelectric phase (space group *P6$_3$cm*). Furthermore, the ferromagnetic order should be retained, so one can classify this material as a potential multiferroic compound [22,31]. The h-$LuFeO_3$ structurally is analogous to another multiferroic compound, the hexagonal $YMnO_3$. However, $YMnO_3$ suffers from extremely low polarization as well as low magnetic transition temperature $T_N \sim 80$ K, and as such it is unfit as a room temperature multiferroic. In the case of h-$LuFeO_3$, the magnetic transition temperature has been reported to increase when the Mn ions are replaced by the Fe ions, while the Lu ions provide higher polarization and Tc values as compared to Y ions [32–35]. However, while promising h-$LuFeO_3$ compound also possesses significant drawbacks. Mainly the fact that the hexagonal phase is metastable in the $LuFeO_3$ matrix and some external factors need to be present [36]. Two main approaches are used in order to stabilize the hexagonal crystal structure. The first one is the use of strain during the formation of thin films, however, the addition of strain as well as interface effects provide additional changes in the properties which can be hard to investigate properly [34,37,38]. The second approach focuses on chemical doping, by either replacing Lu ions with smaller ones (*e.g.* Sc, Co ions) or Fe ions with other ions (*e.g.* Mn, In). Chemical doping with Sc ions in particular has shown great promise [39–42]. It is also worth noting that there have been reports of other rare earth ferrites, that were stabilized in the hexagonal phase such as $ReFeO_3$ (Re = Yb, Er, Ho, Dy, Tb). This has been doe similarly as in the $LuFeO_3$ by means of doping or

strain engineering. However, in most cases even lower T_N values were observed and lutetium ferrite has so far showed the most promise [43,44]. While this approach helps to obtain bulk h-$LuFeO_3$ it also may provide improvement in the polarization values as well as providing changes to both structural and magnetic properties. However, since the hexagonal phase is metastable, it is quite sensitive to preparation conditions, grain microstructure, synthesis method, and the type of chemical dopants and their concentration.

Because of the mentioned arguments, we provide additional fundamental practical insights into the stabilization of the h-$LuFeO_3$ by means of Sc doping. Room temperature crystal structure was investigated by X-ray diffraction and Raman spectroscopy. Particle size and morphology were investigated using scanning electron microscopy. The effects of Sc content on the paraelectric-ferroelectric phase transition were investigated by employing *in-situ* high temperature X-ray diffraction coupled with Rietveld refinement. Magnetic properties were investigated for samples with different Sc content in the temperature range of 4 – 300 K.

2. Experimental part

For the synthesis of $Lu_{(1-x)}Sc_xFeO_3$, Lu_2O_3 (99.99 %, Sigma Aldrich), Sc_2O_3 (99.9 %, Sigma Aldrich), $Fe(NO_3)_3 \cdot 9H_2O$ (98 %, Alfa Aesar), ethylene glycol (EG, Lach-ner), and concentrated HNO_3 (Lach-ner) were used. The synthesis procedures were performed to always obtain a mass of 1 g of the final product. $Lu_{(1-x)}Sc_xFeO_3$ compounds with x = 0.00, 0.15, 0.25, 0.50, 0.55, 0.60, 0.65, 0.75, and 1.00 were prepared. Firstly, Sc_2O_3 was dissolved in concentrated HNO_3 (25 mL) at 200 °C under constant magnetic stirring in a beaker covered by a watch glass. When a clear solution was obtained, Lu_2O_3 was added and dissolved. The Sc and Lu ratios were set depending on the desired final composition. When the added Lu precursor had dissolved, iron nitrate was added in a ratio of 1:1 to the sum of Lu and Sc moles and the solution was diluted to

50 mL with distilled water. The solution cooled down to 150 °C and then stirred for 1 h, after which ethylene glycol was added in a ratio of 1:1 to the metal (Fe + Lu + Sc) ions. The solution with ethylene glycol and the precursor ions was stirred at the same temperature for 1 more hour. Lastly, the watch glass was removed, and the temperature was raised to 220 °C in order to evaporate residual water and to obtain a viscous gel. The beaker with the formed gel is transferred to a drying furnace and dried overnight at T ~ 180 °C. The dried gel was then ground in an agate mortar and annealed at T ~ 1100 °C for 1.5 h with a heating rate of 1 °C/min. The annealed samples were once again ground and further heated at 1300 °C for 3 h with a heating rate of 5 °C/min and finally used for characterization. Synthesis schemes as well as annealing programs can be found in Fig.1.

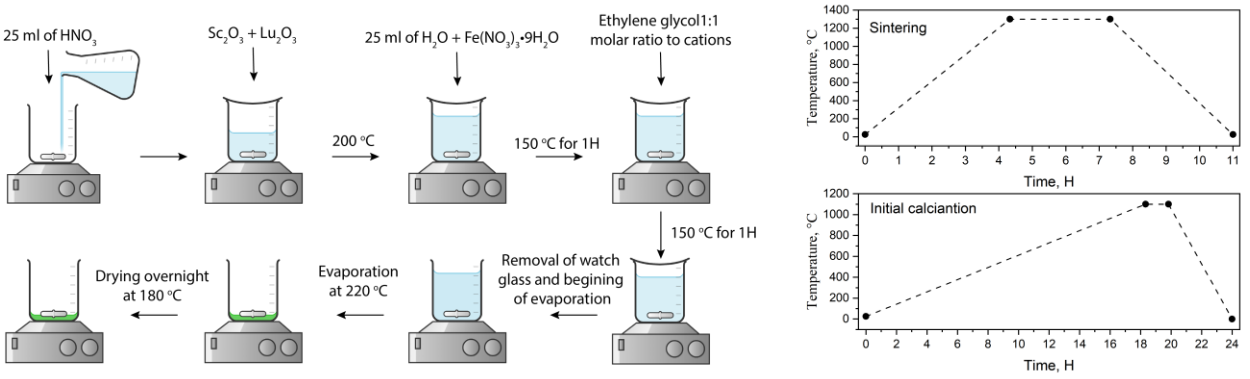

Fig.1. Synthesis scheme (left) and heating conditions (right) of $Lu_{(1-x)}Sc_xFeO_3$ ($0 \leq x \leq 1.00$) compounds.

The XRD measurements were carried out on a Bruker D8 Discover powder diffractometer in the Bragg−Brentano geometry. The diffractometer was equipped with a front monochromator (CuKα1 wavelength λ = 1.5405598 Å) and a LynxEye linear detector discriminating in energy. Temperature dependent measurements were carried out from 30 to 1200 °C (from 100 to 900 °C a step of 100 °C was used while from 900 to 1200 °C a step of 50 °C was used). All of the obtained diffraction patterns were further refined using FullProf software [45]. Raman scattering measurements were conducted using inVia Raman (Renishaw,

United Kingdom) spectrometer equipped with a thermoelectrically cooled (-70 °C) CCD camera and microscope. Raman spectra were excited with a 532 nm beam from the CW diode pumped solid state (DPSS) laser (Renishaw, UK). To avoid damage to the sample, the laser power at the sample was restricted to a very low value, 0.4 mW. The 20x/0.40 NA objective lens and 1800 lines/mm grating were used during all the measurements. The overall integration time was 800 seconds. The position of the Raman bands on the wavenumber axis was calibrated by the polystyrene film standard spectrum. Parameters of the bands were determined by fitting the experimental spectra with Gaussian-Lorentzian shape components using GRAMS/A1 8.0 (Thermo Scientific, USA) software. Scanning electron microscopy micrographs were taken using SEM SU-70 (Hitachi, Japan) with an accelerating voltage of 5kV and a magnification of 5k. Particle size histograms were obtained by randomly measuring 100 different particles using open-source ImageJ software [46]. The magnetic studies were carried out with a SQUID magnetometer (Quantum Design MPMS3) covering the temperature and field range of 2–300 K and ±7 T respectively. The X-ray photoelectron spectroscopy (XPS) analysis was done using a Kratos Axis Supra spectrometer with a Al Kα source (25 mA, 15 kV). The instrument work function was calibrated to give a binding energy (BE) of 83.96 eV for the Au 4f7/2 line for metallic gold and the spectrometer dispersion was adjusted to give a BE of 932.62 eV for the Cu 2p3/2 line of metallic copper. Spectra were analyzed using CasaXPS software.

3. Results and Discussion

3.1. Room temperature X-ray diffraction analysis

In order to investigate the viability of the sol-gel synthesis method for the preparation of $LuFeO_3$ compounds doped with Sc as well as the phase transitions that occurred in this system, the X-ray diffraction analysis coupled with Rietveld refinement procedure was performed for all

of the obtained samples. The diffraction patterns measured at room temperature and refined using the Rietveld method are presented in Fig. 2 and Fig. S1. The crystal structure of the initial $LuFeO_3$ compound is characterized by the orthorhombic symmetry described by the space group *Pnma* (#62) [19,30]. The mentioned symmetry is caused by a rotation of oxygen octahedra due to the different ionic radii of the constituent ions in the perovskite lattice which leads to a disruption of the ideal cubic perovskite symmetry and results in a stabilization of the orthorhombic distortion [47]. The results of structural investigations have confirmed the phase purity of the compounds, and the crystal structure of the samples corresponds to that mentioned in the previous studies [22,31,36,48]. Furthermore, the calculated unit cell parameters (see Fig. 2) are quite similar to those reported in the literature [29,49].

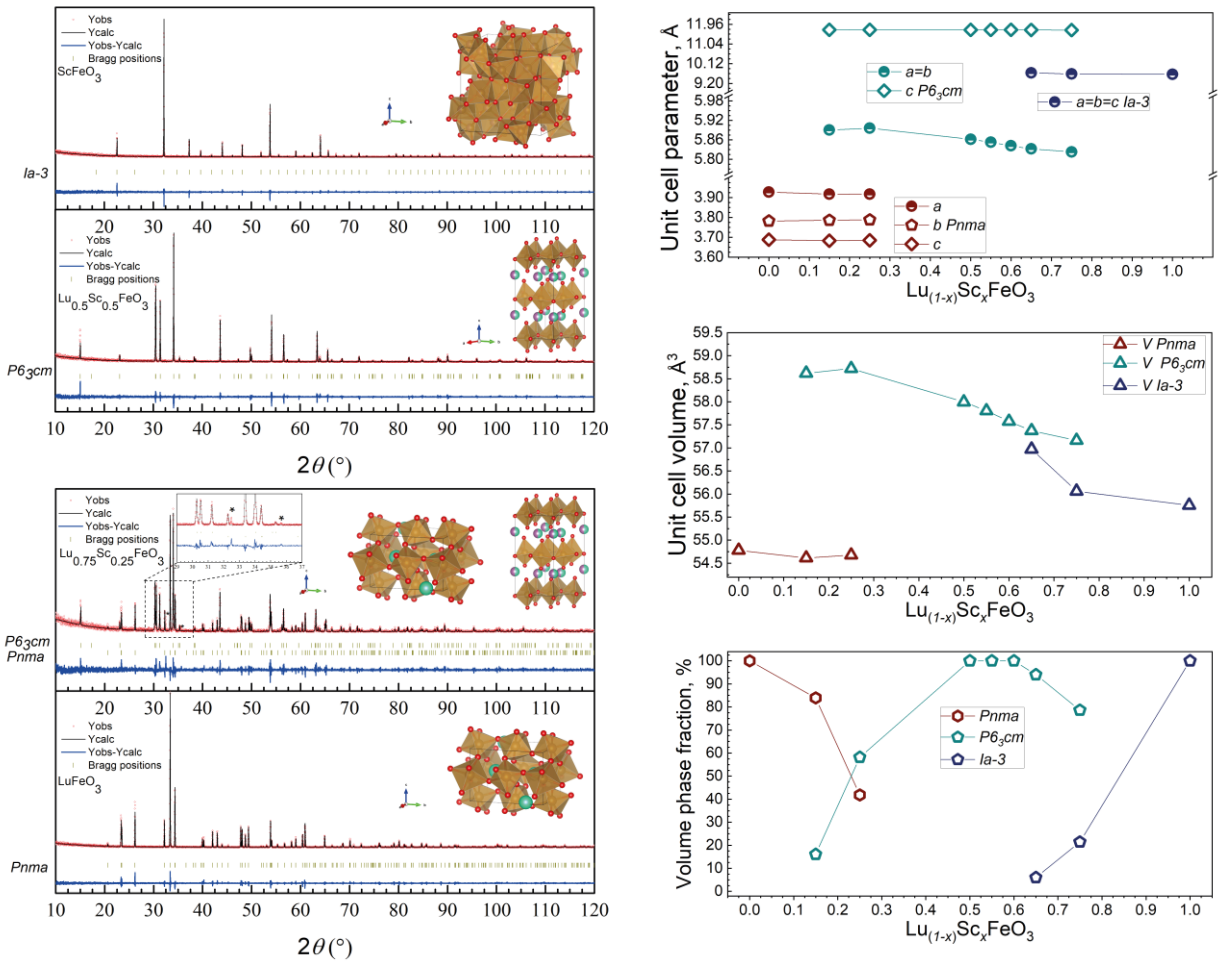

Fig. 2. XRD patterns recorded for $Lu_{(1-x)}Sc_xFeO_3$ ($0 \leq x \leq 1.00$) compounds at room temperature (left). Unit cell parameters, unit cell volume, and volume fraction of the structural phases were calculated for the compounds $Lu_{(1-x)}Sc_xFeO_3$ based on the XRD data at room temperature (right).

From the Rietveld refinement of the XRD patterns, the compounds $Lu_{1-x}Sc_xFeO_3$ with $x < 0.15$ are single phase with orthorhombic structure. For compounds with $x \geq 0.15$, a hexagonal phase, space group *P6₃cm* (#185), can be identified along with it [36,48]. The formation of the hexagonal phase is confirmed by the appearance of the new specific reflections in the diffraction patterns, the most prominent ones are indexed as 002 and 112 and located at $2\theta \approx 15°$ and $2\theta \approx 34°$ respectively (Fig. S1). The hexagonal phase becomes dominant in the compound with $x = 0.25$ wherein its volume fraction reaches 58%, while in the compound with 15% of Sc doping, the hexagonal phase fraction is only about 17% (see Fig. 2). The mentioned hexagonal

phase is considered to be metastable, as it is quite sensitive to the synthesis conditions [36]. The structure of the hexagonal phase is analogous to that observed in a well-known hexagonal compound $YMnO_3$. This structure is not considered to be a perovskite structure as the coordination of the iron ions is changed from 6 coordinated octahedrons to a trigonal bipyramid with 5 oxygen cations in the nearest environment [32,50]. For the compounds doped with 15% and 25% Sc content, some additional low intensity reflections were observed, that cannot be described by either $P6_3cm$ or *Pnma* space groups (Fig. 2, Fig. S1, marked by the asterisks symbols). The intensity of these extra reflections is quite small which hampers an identification of the related phase while its volume fraction is definitely less than 3% and its chemical composition refers to the Lu oxide family.

For the compound with x = 0.5, the crystal structure becomes a single phase with hexagonal symmetry and it can be described by the aforementioned space group $P6_3cm$. This structural state is confirmed by the results of the Rietveld refinement wherein all the reflections were well fitted using the chosen structural model and no additional reflections were observed (see Fig. 2). A similar structural state is observed for the compounds doped with 55% and 60% of Sc, as no additional reflections were observed confirming the single phase character. However, when x reaches 65% and above the diffraction patterns of the related compounds show notable changes, *viz.* several new reflections were observed. These reflections were attributed to the crystal structure of $ScFeO_3$ – the end member of the solid solution row. Its crystal structure is ascribed to the so-called bixbyite structure with cubic symmetry described by the space group *Ia-3* (#206) which is mostly found in simple oxide Mn_2O_3 [51,52]. The aforementioned structure is also not a perovskite structure as the Sc and Fe ions are quite similar in size and the discrete perovskite positions are unlikely to be maintained. This structure is notably identified by the

main specific *(222)* and *(400)* reflections located at $2\theta \approx 31.9°$ and $2\theta \approx 37.0°$ respectively. However, it is worth noting that according to the refinement results the volume fraction of this cubic phase is quite small (~ 6%) in the compound with $x = 0.65$ (see Fig. 2.). Upon further increase in the Sc concentration, the volume fraction of the bixbyite phase increases: in the compound with x = 0.75 the volume fraction of the cubic phase reaches 21%. It is worthy to note that the annealing temperature notably affects the structural state of the compounds in the way as described below. High annealing temperature, i.e. 1300 °C and above, fosters a formation of both hexagonal and cubic phases in the compounds with lower Sc content as compared to the case when the compounds were prepared at lower temperatures [53]. For example, structural state of the two phase compound with $x < 0.5$ prepared at T ~ 1100 °C is characterized by a notably lower volume fraction of the hexagonal phase [53] thus one can conclude that high temperature synthesis provides a stabilization of the hexagonal phase accompanied with notable changes in the grain morphology as confirmed by SEM analysis presented in the next section. When Lu ions are fully replaced by Sc ions the single phase bixbyite structure stabilizes as confirmed by the Rietveld refinement. Furthermore, in some instances there have been reports on the stabilization of hexagonal phase at low (below 1000 °C) synthesis temperatures with single phase $LuFeO_3$ or when it is slightly doped with rare earth elements. However, larger additions of both Ho and La have led to stabilization of the orthorhombic LufeO3 and disappearance of the hexagonal phase [29,54]. Additionally, there have been reports on other hexagonal rare earth ferrites, in particular the hexagonal variant of $YbFeO_3$ was also stabilized by Sc doping. However in this case a larger amount of Sc doping (60 % and above) needed to obtain a single phase hexagonal structure, and in some cases impurities of ytterbium iron garnet were also observed [44].

The evolution of the unit cell parameters, the unit cell volumes as well as the volume fractions of the constituent phases as a function of Sc doping are given in Fig. 2 as well. In the case of the orthorhombic phase, the *a*- and *c*- parameters reduce upon the chemical doping up to 15%, while the *b*- parameter slightly increases. However, when x is increased to 0.25 all the unit cell parameter values slightly increase. This modification is quite unusual as a simple contraction of the unit cell is expected because of the difference in the ionic radii of Sc^{3+} (0.87 Å) and Lu^{3+} (0.977 Å). While the obtained results show a decrease in the unit cell volume, the unit cell is additionally and unevenly distorted upon the Sc doping. The structure of the compounds with the hexagonal phase shows even more pronounced anomalies and uneven changes in the cell parameters. While both the *a*- and *c*- parameters decrease (Fig. 2), (the sample doped with 15% of Sc is the only exception as its *a*- parameter has a larger value as compared to that specific to the sample doped with 25% of Sc); the rate of these changes is much larger in the case of the *a*-parameter. Assuming the entire doping range attributed to the hexagonal phase the reduction in the *a*-parameter is about one order of magnitude more as compared to that calculated for the *c*-parameter, thus resulting in an increase of the *c/a* ratio. It should be noted, that the mentioned distortion of the crystal lattice is quite unusual, however, it may potentially be quite beneficial as in some reports the room temperature multiferroicity may be realized in the case when the *c/a* ratio reaches about 2.15 [31]. In the case of the polar structure described by the space group $P6_3cm$, the unit cell volume decreases quite linearly and there are no significant discrepancies from this trend.

Discussing the unit cell parameters of the bixbyite phase one can see an expected decrease in the unit cell volume without any significant deviation as the unit cell contracts because of the difference in the ionic radii of the Lu and Sc ions. The only deviation in the structural parameters

refers to a more pronounced contraction of the unit cell observed in the concentration range $0.65 \leq x \leq 0.75$ as compared to the region $0.75 < x \leq 1$. The mentioned changes in the unit cell parameters and in turn the unit cell volume can be easily confirmed by a notable shift of the diffraction reflections towards higher angles $2\theta°$ (Fig. 2). The concentration driven changes in the volume fraction of the respective structural phases are also presented in Fig. 2. There are 5 different phase composition regions that can be denoted depending on the Sc content. The first region is related to the section specific to the orthorhombic phase only and this structural state is stable in the concentration range of $0 \leq x < 0.15$. The second region is related to a mixture of both the hexagonal and the orthorhombic phases and it is located in the concentration range of $0.15 \leq x < 0.40$. This region is followed by a single phase hexagonal one which exists in the range of $0.40 \leq x < 0.65$. The fourth phase region refers to a mixture of the phases described by the space groups $P6_3cm$ and *Ia-3* and it exists in the range of $0.65 \leq x \lesssim 0.90$. The final region is attributed to the cubic bixbyite phase, and it exists in the range of $0.90 \lesssim x < 1.00$. It is also worthy to note that the phase boundary ranges are quite difficult to estimate precisely because of a number of internal (grain size, morphology, etc.) and external (synthesis conditions) factors. The changes in the phase volume fractions are gradual with the Sc doping thus indicating high chemical homogeneity of the compounds as well as the viability of the sol-gel preparation method for the studied compounds.

3.2. Room temperature Raman spectroscopy

Raman spectroscopy provides a possibility to acquire molecular level information on short-range structure, bonding, symmetry on a local scale level, and disorders of the compounds under investigation; this is important additional information difficult to obtain by other methods [55–59]. Fig. 3 shows Raman spectra of polycrystalline $LuFeO_3$ and $ScFeO_3$ compounds

prepared by annealing at 1300 °C. Group theory analysis predicts 24 first-order Raman active modes for orthorhombic $LuFeO_3$ which are distributed by the symmetry in the following way: $7A_g$, $5B_{1g}$, $7B_{2g}$, and $5B_{3g}$ [53]. The characteristic A_g bands of $LuFeO_3$ are located at 108, 133, 276, 432, 451, and 516 cm^{-1}; while well-defined B_{2g} bands are visible at 158 and 349 cm^{-1} [53]. The bands located at frequencies higher than 600 cm^{-1} contain a contribution from second-order vibrational modes [53]. Thus, an intense and broad band at 1305 cm^{-1} is associated with the overtone of oxygen stretching vibration [60,61]. Raman bands below 200 cm^{-1} can be visualized as associated mainly with vibrations of heavy rare-earth ions; those in the frequency region 200 – 350 cm^{-1} can be linked with tilting motions of FeO_6 octahedrons; the modes in the region 350 – 500 cm^{-1} are associated mainly with bending vibrations of oxygen atoms and stretching vibrations of Fe–O bonds take place at frequencies higher than 500 cm^{-1} [55]. It should be noted that the peak positions of our sample are very close to Raman spectrum of single crystal $LuFeO_3$ [56] indicating high crystal quality of the studied compound. The Raman spectrum of $ScFeO_3$ is dominated by strong feature at 411 cm^{-1} and well-defined first-order bands at 165 and 509 cm^{-1} (Figure 1). X-ray diffraction studies revealed bixbyite structure with cubic symmetry (*I-a3* space group). Such structure exhibits an intense Raman band of F_g symmetry [53,62]. In the case of $ScFeO_3$ compound, this band is visible near 411 cm^{-1}. Two other lower intensity bands located near 509 and 289 cm^{-1} also belong to the F_g symmetry modes. The narrow low-frequency band at 165 cm^{-1} most likely belongs to E_g symmetry vibrational mode [53,62]. The Raman bands located at frequencies higher than 500 cm^{-1} contain a high contribution from second-order phonons. In particular, the broad feature near 1292 cm^{-1} is related to the overtone of oxygen stretching vibration [60,61,63].

Composition-dependent Raman spectra of $Lu_{(1-x)}Sc_xFeO_3$ compounds are shown in Fig. 4.

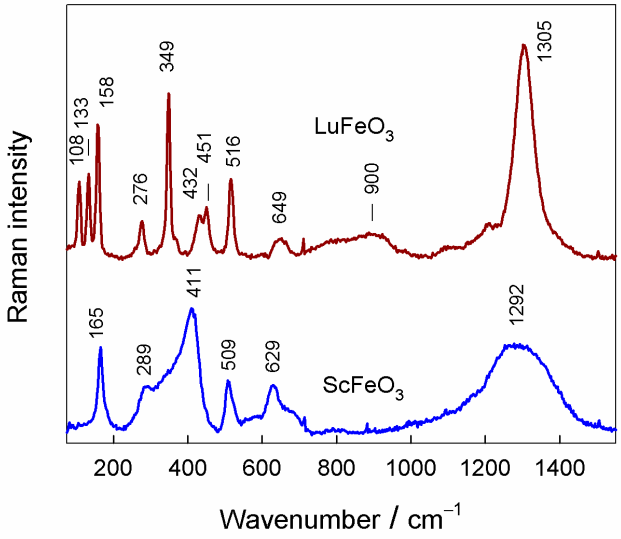

Fig. 3. Raman spectra of polycrystalline $LuFeO_3$ and $ScFeO_3$. The annealing temperature is 1300 °C. The excitation wavelength is 532 nm (0.4 mW).

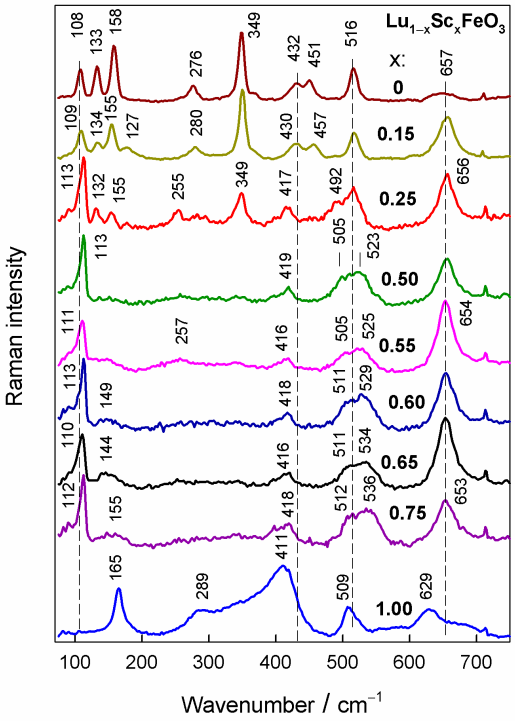

Fig. 4. Composition dependent Raman spectra of polycrystalline $Lu_{(1-x)}Sc_xFeO_3$ compounds. The annealing temperature is 1300 °C. Intensities are normalized to the intensity of the most intense band and spectra are shifted vertically for clarity. The excitation wavelength is 532 nm (0.4 mW).

Even a small amount of Sc^{3+} ions ($x = 0.15$) results in observable changes in the Raman spectrum; the relative intensity of the prominent 134 (A_g) band decreases and a new low-intensity band appears at 127 cm^{-1}. In addition, the relative intensity of the high frequency band near 657 cm^{-1} increases. These spectral changes are consistent with perturbations of the lattice parameters. The most significant changes in the low frequency region indicate perturbations in the motions of heavy rare-earth ions because of presence the of Sc^{3+}. The intensity of high frequency band at 657 cm^{-1} is very sensitive to defectivity in the vicinity of FeO_6 octahedra. An increase in Sc^{3+} concentration to x = 0.25 results in drastic changes observed in the Raman spectrum. The relative intensity of characteristic low frequency modes decreases, and new

vibrational features at 255, 417, and 492 cm^{-1} appear. The observed spectral changes indicate the coexistence of two different phases. Further increase in the content of Sc^{3+} ions results in spectral disappearance of the initial phase. The new structural phase dominates in the concentration range from x = 0.50 to x = 0.75. Perturbations in the lattice of this phase show an increase in the frequency of 523 cm^{-1} band to 536 cm^{-1} and the appearance of a broad low-intensity band near 155 cm^{-1}. Overall, the obtained results of Raman spectroscopy quite closely correlate to the XRD data. The obtained phases and their concentration stability regions match quite confirm the ones obtained by analyzing XRD data. Mainly the existences of the single phase orthorhombic region, a mixture of orthorhombic and hexagonal regions, a single phase hexagonal region, then a mixture of the cubic and hexagonal phases, and lastly a single phase cubic region are confirmed.

3.3. Temperature dependent X-ray diffraction analysis

Analysis of the temperature-dependent diffraction data obtained for $LuFeO_3$ points at the phase transition from the low temperature polar phase (space group $P6_3cm$) to a high temperature non-polar phase (space group $P6_3/mmc$, #194) similar to that, observed in $YMnO_3$ [27,35]. The structural transition is also important in order to investigate a correlation between the structure and electrical and magnetic (magnetoelectric) properties of the compounds. The related diffraction patterns are presented in Fig. 5 and Figs. S2 and S3. Examination of the diffraction patterns obtained for the initial compound $LuFeO_3$ did not reveal any additional reflections at elevated temperatures thus confirming the absence of structural changes in the measured temperature range. A gradual shift of the diffraction peaks towards lower angles observed with a temperature increase is caused by the thermal expansion of the crystal lattice of the compound.

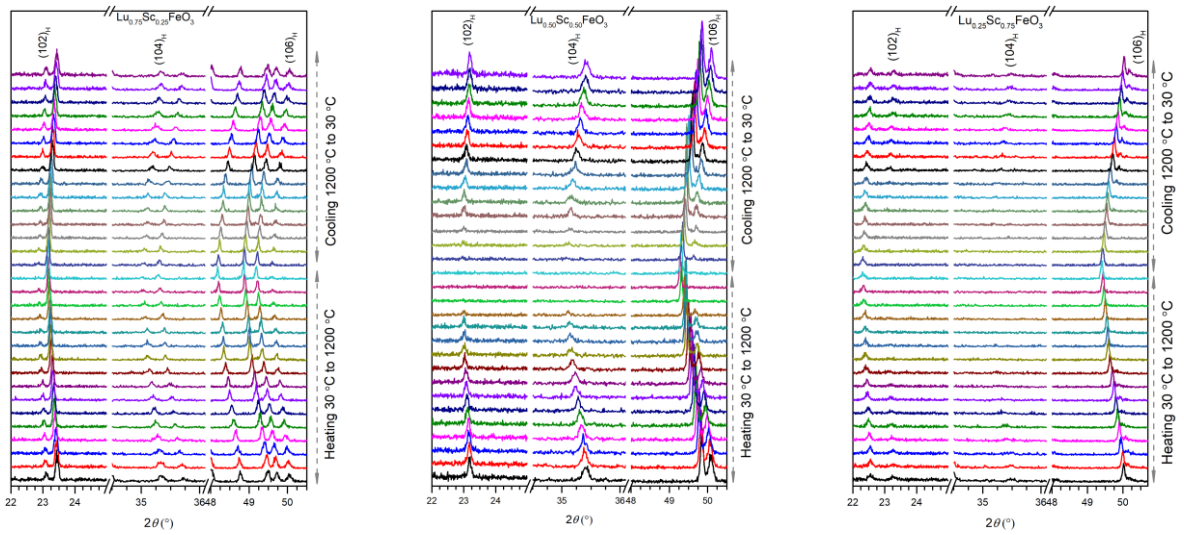

Fig. 5. Temperature dependent XRD patterns of $Lu_{(1-x)}Sc_xFeO_3$, when x = 0.25, 0.50, and 0.75.

However, it is worth noting that the reflections *002* and *210* located at $2\theta \approx 34.1°$ exhibit a splitting upon a temperature increase which is caused by the different trends in a modification of the unit cell parameters, viz. the c – parameter increases more rapidly with temperature increase as compared to the changes observed for the a- and b- parameters. For the compound with x = 0.15, no significant changes were observed during heating, which can be caused by the small fraction of the hexagonal phase present in the sample. Thus, only a shift of the reflections towards lower angles at higher temperatures was observed. In the compound with x = 0.25 with the mixed structural state in which the fraction of the hexagonal phase is higher, an increase in temperature leads to a shift in the ratio between the coexisting structural phases as can be seen by the modification of the specific reflections. Particularly, the intensity of the reflections specific for the $P6_3cm$ polar phase decreases upon temperature increase, viz. the reflections *(102)*, *(200|104)*, and *(106)* located at $2\theta \approx 23.0°$, 35.3° and 50.0° respectively [27]. The phase transition to the non-polar hexagonal structure is not completed up to T ~ 1200 °C - the highest temperature achieved in the experiments (Fig. 5). Analysis of the diffraction patterns recorded

for the compounds with the single phase hexagonal structure ($0.50 \leq x < 0.65$) has allowed to estimate a modification of the structural state as a function of temperature. Thus, the intensity of the reflections *(102)*, *(200|104)*, and *(106)* decreases in intensity with temperature increase and become almost negligible at temperatures above ~ 1100 °C, thus denoting a stabilization of the non-polar hexagonal phase described by the space group $P6_3/mmc$. The modification of the structural state estimated for the compounds with x = 0.55 and x = 0.6 resembles that observed for the compound with $x = 0.5$, while a decrease in the intensity of the reflections specific of the polar hexagonal phase occurs at lower temperatures, viz. at ~ 1050 °C and 1000 °C for the compounds with $x = 0.55$ and 0.6 respectively. Thus, the temperature of the structural transition to the non-polar hexagonal phase decreases with Sc concentration and for the compound with $x = 0.65$, it is about 950 °C while for the compound with $x = 0.75$, it decreases down to about 800 °C. The structural state of the extreme member of the solid solution ($x = 1$) does not exhibit any changes in the structure in the whole measured temperature range as confirmed by the diffraction data obtained upon heating and cooling cycles.

A discrete trend in the structure change is ascribed to the phase transition from the polar phase $P6_3cm$ stable at room temperature to the high temperature non-polar $P6_3/mmc$ structure. From the given results it is evident that the amount of Sc ions introduced into the unit cell notably lowers the transition temperature. The mentioned tendency is accurate for the compounds regardless of their structural state (single phase or mixed) at room temperature.

The data denoting an evolution of the unit cell parameters, the unit cell volume and the different structural phases is presented in the Figs. S4-S7. For the undoped compound $LuFeO_3$, a linear increase in the unit cell parameters is observed, though the *c*- parameter increases more rapidly as compared to the evolution of the *a*- or *b*- parameters. The increase of the *c*- parameter

was calculated to be at 1.5% while for the *a*- and *b*- parameters it is only 0.97 and 1.4% respectively. The positions of the aforementioned reflections, viz. *(002)* and *(210)* are shifted in different directions which confirms the uneven increase in the unit cell parameters. Most likely, that different character in the modification of the unit cell parameters is caused by a specific rotation of the oxygen octahedra. The noted phenomenon is observed for the Sc doped compounds with the polar hexagonal phase. In the case of the *a*-parameter, it increases linearly during both the cooling and heating cycles. The increase of the parameter upon heating and its decrease for the same value upon cooling indicates the stability of the existing phase, additionally, the parameter values do not intersect nor overlap over all of the Sc doping concentration range.

A different tendency is observed in the case of the *c*- parameter, as its value increases nonlinearly upon temperature increase and this tendency is present for all of the hexagonal compounds. When the temperature reaches 300 °C the *c*- unit cell parameter becomes almost identical for all of the samples. And when the temperature is increased further the compound with x = 0.25 shows the lowest value, while the compound with x = 0.75 shows the highest value. Such temperature driven distortion is peculiar as ordinarily an exactly opposite situation should occur, however in this case the expansion along the *c* axis is much more pronounced for higher Sc content. In the case of the compounds with a fraction of the cubic bixbyite phase ($x = 0.65$, 0.75 and 1.00) there are no significant changes in the parameters observed upon temperature change. In all cases the unit cell expansion was observed at the elevated temperatures, however, the increase in the unit cell parameters was calculated to be linear and a homogenous expansion was concluded.

Assuming the results of the structural analysis a preliminary temperature dependent phase diagram has been constructed as seen in Fig. 6.

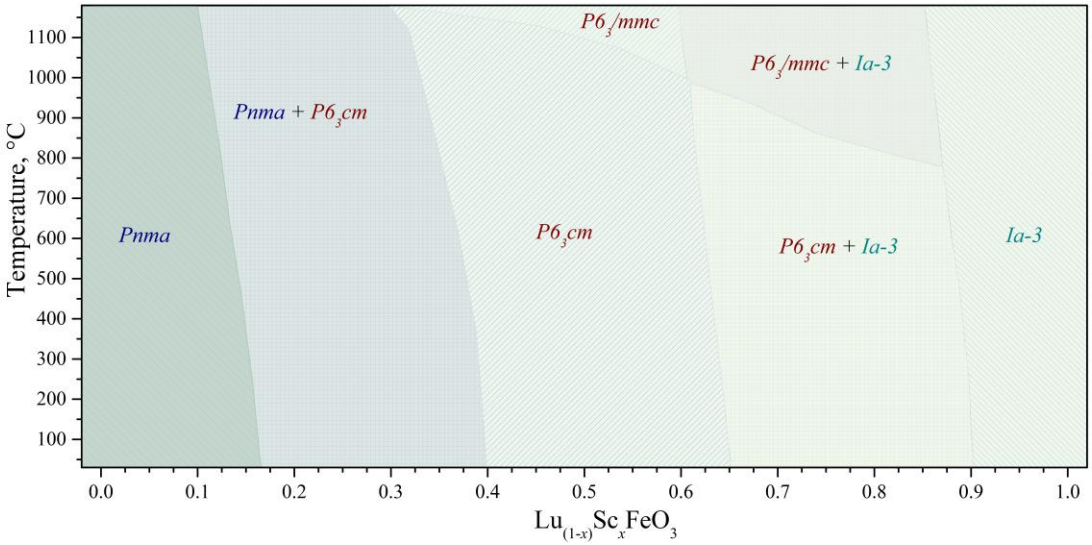

Fig. 6. Temperature driven phase diagram for the compounds $Lu_{(1-x)}Sc_xFeO_3$ based on the Rietveld refinement of XRD data obtained at different temperatures.

While the hexagonal phase described by the space group *P6₃cm* remains stable in the compounds of the middle Sc concentration range, at high temperatures the transition to the non-polar hexagonal phase described by the space group *P6₃/mmc* occurs. In the case of the compound with $x = 0.5$, this transition occurs at 1150 °C. As mentioned before, the temperature of the phase transition from the polar hexagonal phase to the non-polar hexagonal phase decreases upon the increase in Sc content, the same tendency is observed for the transition from the hexagonal to the cubic phase (Fig. 6). It is quite difficult to estimate correctly the temperature of the transition from the polar to the non-polar phase, as most likely any further increase in Sc content would lead to the formation of the single phase cubic structure. Furthermore, it is worth noting that in the compounds with a mixed structural state (*e.g.* $x = 0.15$, 0.25, 0.75) the volume fraction of each structural phase remains nearly the same, independently of the temperature. This

indicates that the phase formation equilibrium has been reached for this temperature. When the phase transition temperature is reached for the mixed phase samples, the volume fractions of the phases remain the same and only the $P6_3cm$ to $P6_3/mmc$ transition occurs. In conclusion of the temperature-dependent XRD study, a dependence of the polar to non-polar transition temperature of Sc content was evidenced while also identifying the exact phases coexisting in the phase boundary region. Finally, this study provided new insight into the evolution of the unit cell, especially along the *c*-axis at temperatures above 300 °C.

3.4. Scanning electron microscopy

In order to track the effects of Sc doping accompanied by the concentration-driven phase transitions that occurred at room temperature on the particle size and their morphology the SEM measurements have been performed (Fig.7). The software Image-J was used for the analysis of the particle size and thereafter to construct the particle size histograms as a function of the Sc content [46]. The undoped $LuFeO_3$ compound consists of semi-spherical particles with a particle size in the range from 0.5 to 6.5 μm, the average value is ~2.726 μm. The introduction of 15% of Sc into the structure does not lead to any significant changes in the particle morphology, however, the average size was slightly reduced to ~2.668 μm. Upon further increase of Sc content up to x = 0.25, significant changes were observed. The particle shape became more rectangular as compared to the previous samples, with both the particle size distribution as well as at the average size decreasing. The particle size distribution for 0.25 Sc doped sample was in the range from 0.5 to 3 μm and the average size of the particles decreases to ~1.606 μm. Both the changes in the size and shape may be related to the changes in the crystal structure, as the compound with x = 0.25 is mainly hexagonal as compared to the previous compounds where the orthorhombic phase was dominant. The same trend of decreasing particle size and the narrowing of the particle size distribution range was observed for all compounds with the dominant

hexagonal phase. The average size of the particles in the compounds with x = 0.50, 0.55, 0.60, 0.65 and 0.75 was ~1.322 μm, ~1.283 μm, ~1.172 μm, ~1.053 μm and ~0.962 μm respectively. However, for the compound $ScFeO_3$ a different trend was observed, the particles became more semi-spherical again and, in the compounds, doped with x = 1.0 the average particle size is increased to 1.669 μm.

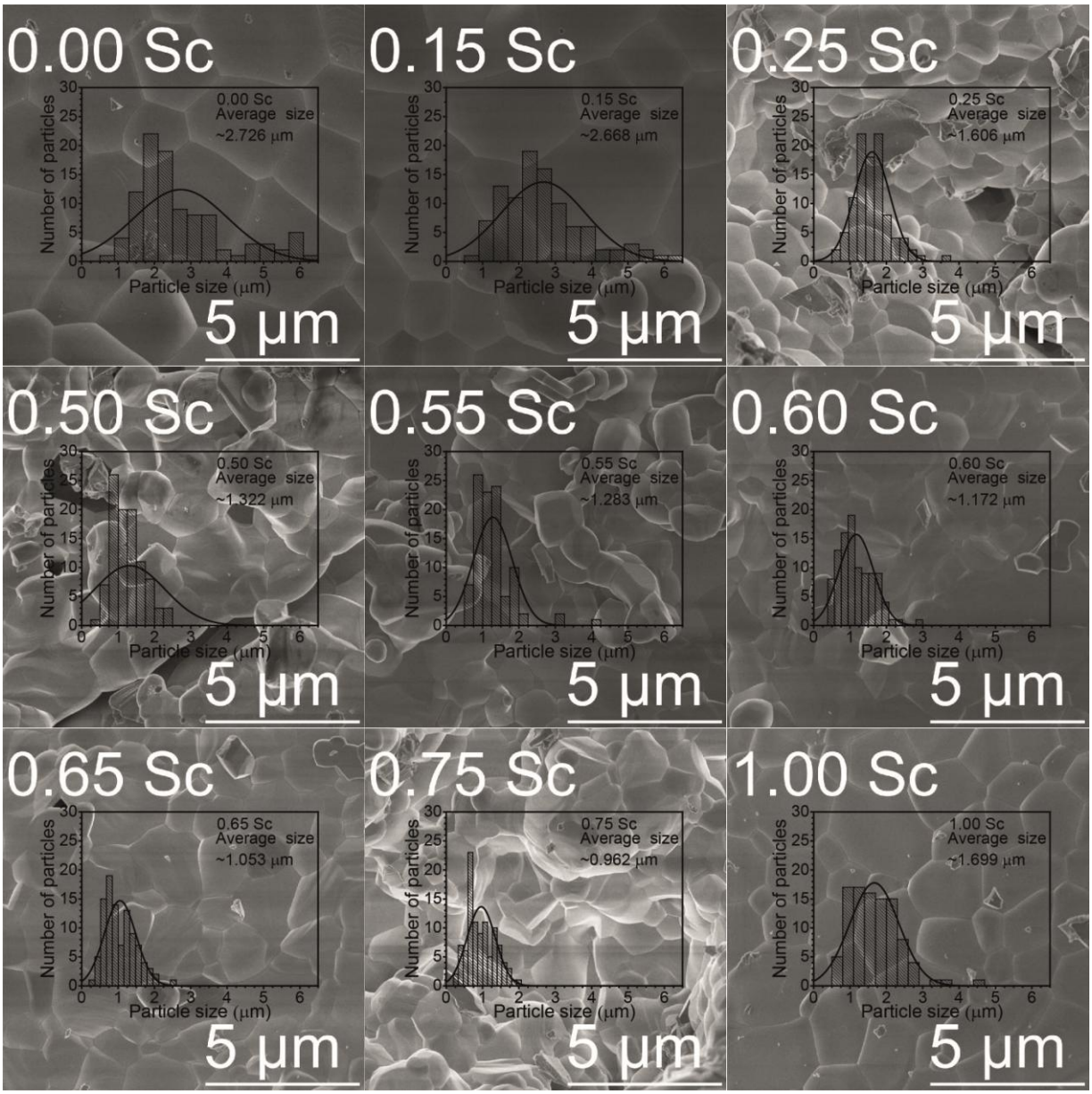

Fig. 7. SEM micrographs of $Lu_{(1-x)}Sc_xFeO_3$ with particle size histograms.

The tendency of decreasing particle size in the compounds with mixed and single phase hexagonal regions was also observed in the samples annealed at 1100 °C in our previous report [53]. Furthermore, the overall particle size after annealing at 1300 °C increased by around a factor of 10 as compared to samples heated only up to 1100 °C, differences in particle morphology between *Pnma/Ia-3* and the $P6_3cm$ can still be observed in both cases [53]. The drastic increase in particle size could be the reason for differences in the phase composition at different annealing temperatures. This may be especially pronounced in the hexagonal structure as it is considered to be metastable in this system and as such much more sensitive to external factors. The relatively broad region of the particle size distribution is also quite common for the compounds prepared by the aqueous sol-gel method and can be found in numerous reports [3,57,64]. Overall, it can be concluded that in the case of the solid solution system $LuFeO_3$-$ScFeO_3$, the particle size and their shape are affected by the structural phase transitions as well as the Sc content, however to a lesser extent.

3.5. X-ray photoelectron spectroscopy

X-ray photoelectron spectroscopy was used in order to estimate the elemental composition as well as the oxidation state of iron ions as it is of high importance for the magnetic properties of the compounds. The chemical composition for all samples was analyzed using low resolution survey scans that can be found in Fig. 8. From the survey spectra, several peaks can be observed. Mainly the Fe 2p peaks at around 720 to 700 eV, and the O 1s peaks at around 530 eV, the Sc 2p peaks from 410 to 390 eV and lastly the Lu 4d and 4f peaks at around 200 and 7 eV respectively. The position of the aforementioned bands is similar to that reported in such systems [65,66]. Furthermore, the content of both Sc and Lu can be tracked quite clearly by accounting for the changes in the intensity of their specific peaks. In the case of Sc, the intensity of the

specific peaks increases as more of Sc is introduced into the sample and the intensity of Lu specific peaks decreases at the same time. As such it indicates that doping was successful. The relative intensity of Fe specific peak remains the same in all samples. The estimation of Fe oxidation state is also quite important as in this system the iron ions are responsible for the magnetic properties of the entire compound and any changes to it could result in magnetic state variance. As such the high resolution scans in the range from 722 to 706 eV were performed. The obtained results can be found in Fig. 9 and Fig. S8.

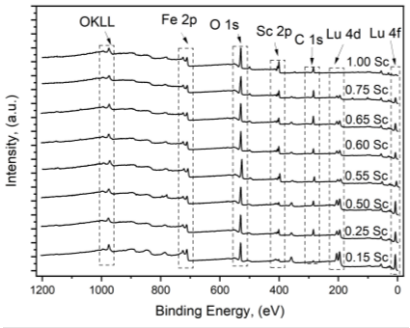

Fig. 8. Wide range survey XPS scans of $Lu_{(1-x)}Sc_xFeO_3$ compounds in the binding energy range from 1200 to 0 eV.

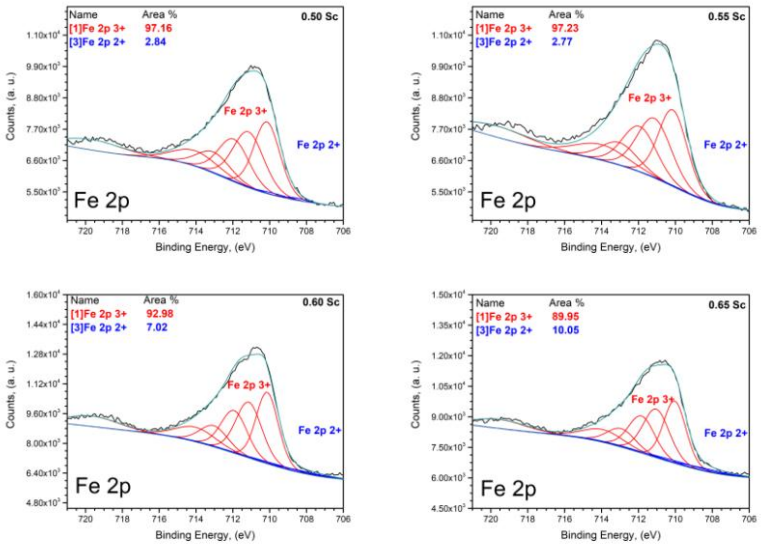

Fig. 9. Fitted high resolution XPS Fe 2p orbital spectra of $Lu_{(1-x)}Sc_xFeO_3$ compounds (x = 0.50, 0.55, 0.60, 0.65) in the binding energy range from 722 to 706 eV.

Interestingly, the peak position in all samples remained the same with a maximum at around 710 eV, this indicates that the local environment for iron remains relatively similar [67]. This is particularly interesting as the coordination environment of iron is different in *Pnma*, $P6_3cm$ and *Ia-3* structures. The relatively broad peak in this case is most likely caused by the spin-orbital coupling in the 2p core and 3d electrons and the effect of the crystal field [68].

Furthermore, in all cases, a small satellite peak at around 720 to 717 eV is caused by the high spin state of the iron. The obtained spectra were also fitted with potential peaks of iron in 3+ and 2+ states. The fitting model was based on calculations done by Gupta and Sen, who have calculated the expected core p level energies for iron ions, as well practical data obtained by other scientists [68–71]. In the fitting model blue curves represent Fe^{2+} state while the red ones the Fe^{3+}state. From the fitting data displayed in the graphs, it can be seen that there are no significant changes in the oxidation state caused by the doping of Sc as it is almost 100% in the 3+ state. This is quite expected as in this case the electronegativity was maintained as a 3+ charge having Lu ion was replaced by Sc with the same ionic charge. As such most likely the changes in magnetic properties were caused fully by the rotation of the iron coordination polyhedron as well as its changes.

3.6. Temperature dependent and isothermal magnetization measurements

The temperature dependent curves of magnetic susceptibility measured at 100 Oe in field cooled (FC) and zero field cooled (ZFC) modes, as well as isothermal magnetization data (Figs. 10-13), show an evolution of the magnetic properties as a function of the Sc content. The temperature dependent magnetization and isothermal magnetization curves obtained for the initial compound $LuFeO_3$ (orthorhombic) are in accordance with the reported canted antiferromagnetic behavior, with T_N = 626 K [72,73]. Here the ZFC and FC do not reach the same value even at high temperature because we could not overcome the ordering temperature. The fact that the coercive fields increase when the temperature increases, somehow counter-intuitive, is in fact due to the fact that even at 7 T the system is far from saturation [72,73]. The maximum coercive field and remnant magnetization are obtained here at 300 K with $\mu_0 H_c$ = 1.3 T and M_r = 0.01 μ_B/f.u.

For $ScFeO_3$, with a cubic Bixbyite structure, the other extreme of the Sc doped series, the magnetic data indicates an antiferromagnetic behavior, as described in the literature [74].

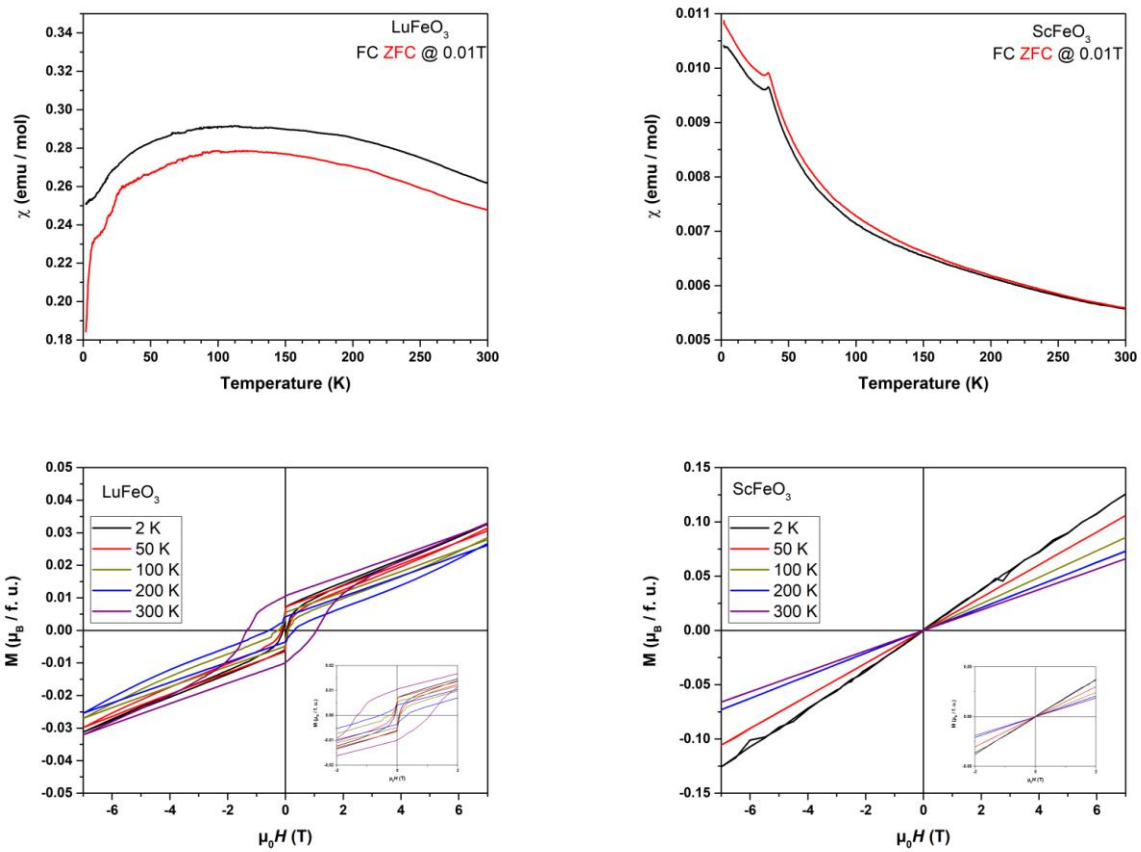

Fig. 10. Magnetic field dependencies obtained at different temperatures (bottom) and FC/ZFC curves (top) of $LuFeO_3$ and $ScFeO_3$.

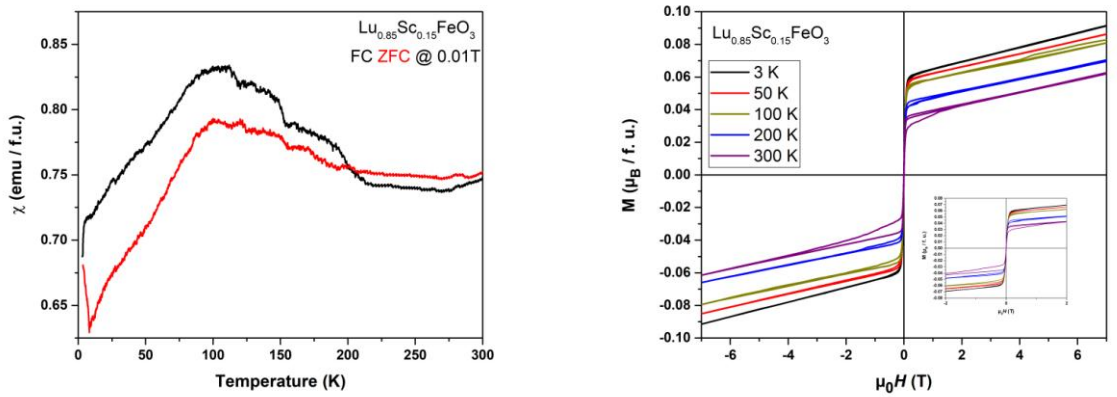

Fig. 11. FC/ZFC curves (left) and magnetic field dependencies obtained at different temperatures (right) of $Lu_{(1-x)}Sc_xFeO_3$ when x = 0.15.

510

511

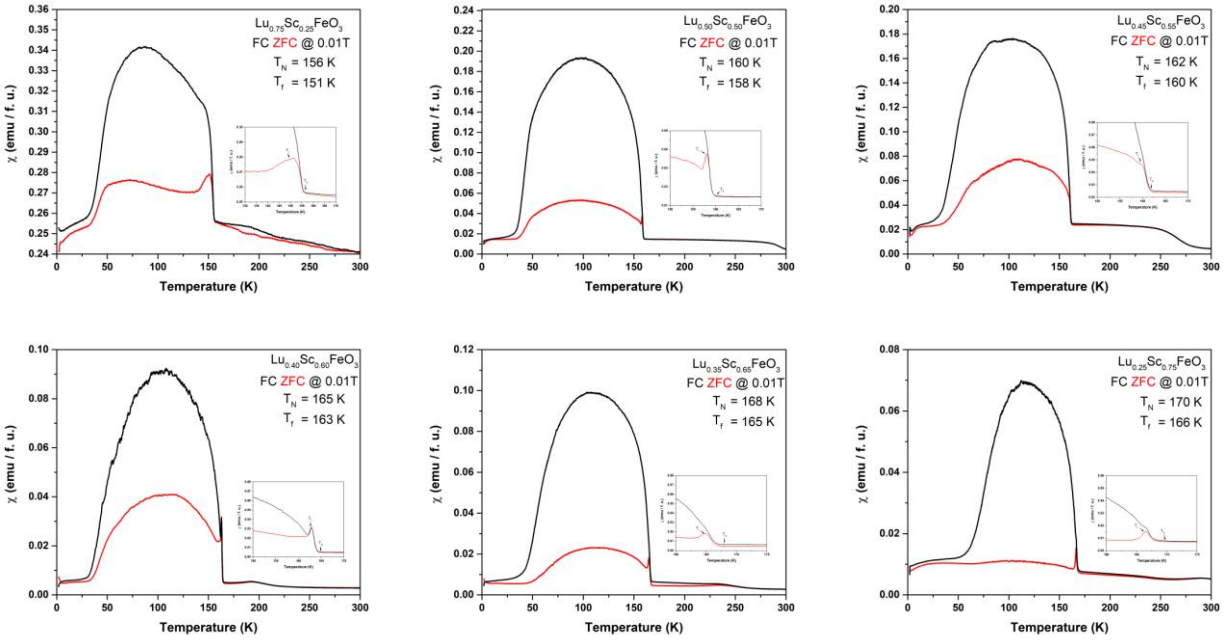

Fig. 12. FC/ZFC curves of $Lu_{(1-x)}Sc_xFeO_3$ when x = 0.25, 0.50, 0.55, 0.60, 0.65, 0.75.

512

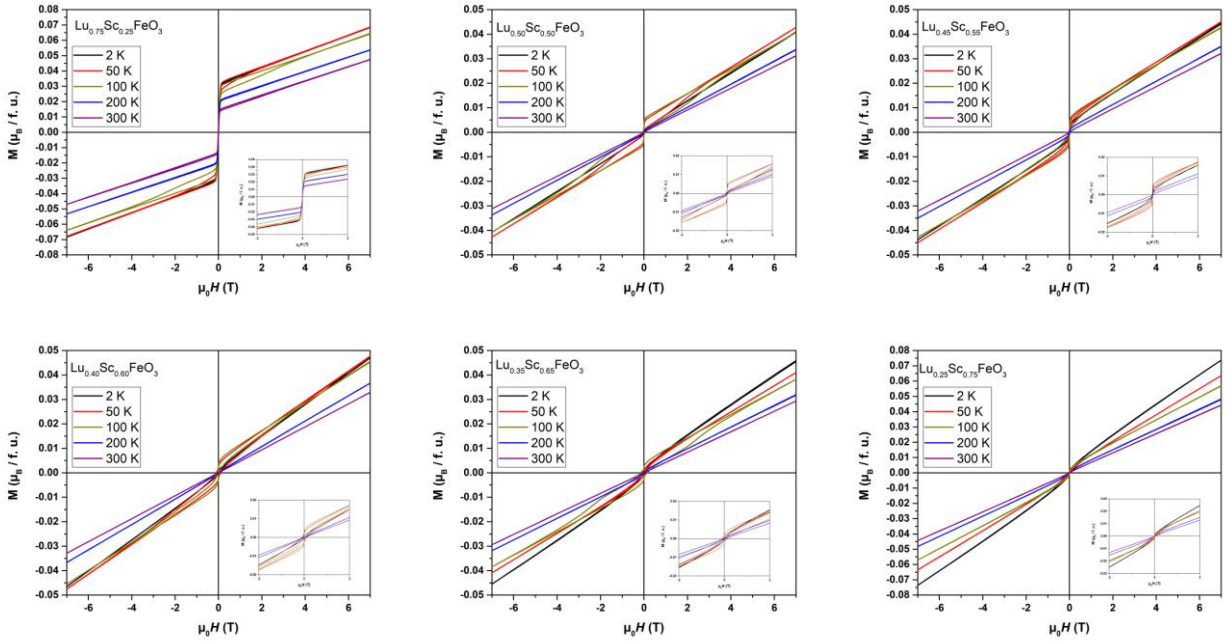

Fig. 13. Magnetic field dependencies obtained at different temperatures of $Lu_{(1-x)}Sc_xFeO_3$ when x = 0.25, 0.50, 0.55, 0.60, 0.65, 0.75.

Chemical substitution of Lu ions by Sc ions leads to notable changes in the structure of the compounds, which is mainly associated with a stabilization of the hexagonal structure and thus a different geometry in the arrangement of the Fe^{3+} ions and their local surrounding. It is known, that in the hexagonal phase, the arrangement of the Fe^{3+} ions forms a 120° triangle spin structure within the a-b plane of the hexagonal lattice [37,75].

Temperature dependent magnetization curves show an abrupt increase of the FC and ZFC curves upon cooling below ~160 K which is observed for the compounds with $0.2 < x < 0.75$, viz. having a dominant hexagonal structure [44]. In the case when x = 0.15 the FC/ZFC curve resembles a superposition of those obtained for orthorhombic and hexagonal structures, most likely due to the presence of both phases in the compound. It should be noted that the critical temperature (T_N) attributed to spin reorientation gradually increases with Sc content which can be ascribed to a strengthening of the exchange interaction between the Fe^{3+} magnetic moments associated with a decrease of the unit cell lattice [76].

A decrease of the magnetization below 100 K observed for the compounds of $Lu_{1-x}Sc_xFeO_3$ with $x \leq 0.75$ is also associated with a spin orientation phenomenon similar to that observed in the initial compound $LuFeO_3$ and discussed above. The temperature dependent magnetization data confirm the presence of non-zero remanent magnetization at temperatures above the mentioned spin reorientation temperature (T_N) and the obtained results are the accordance with the model of the magnetic structure of the $LuFeO_3$-based hexagonal compounds with an AFM transition of about 450 K [76,77]. It is worth noting that similar T_N values were reported in another hexagonal $YbFeO_3$ doped with Sc, of around 165 K, when 0.58 of Sc was used [44]. Furthermore, significantly higher T_N values were reported when In doping was used instead of Scin $LuFeO_3$. In this case the T_N values were as high as 350 to 360 K, thus indicating about a much smaller reduction as compared to undoped $LuFeO_3$ [27].

4. Conclusions

Based on the obtained results it is concluded that a modified ethylene glycol-based Sol-Gel synthesis route can be applied for the preparation of high-purity $Lu_{(1-x)}Sc_xFeO_3$ samples. From the XRD and Raman spectroscopy data 5 different phase composition regions were observed. The first region when $x < 0.15$ is characterized by the orthorhombic structure described by the space group *Pnma*. When the Sc content is $0.15 \leq x < 0.40$ a phase mixture of the phases characterized by the *Pnma* and $P6_3cm$ phases is formed, with the fraction of the hexagonal phase increasing at higher Sc doping values. The hexagonal phase without any secondary phase was stabilized when $0.40 \leq x < 0.65$. An onset of the bixbyite (s.g. *Ia-3*) phase occurs when $x \geq 0.65$, however a phase mix with the polar $P6_3cm$ phase is formed up to $x = 0.90$, followed by the single phase cubic structural region. Temperature dependent diffraction experiments revealed that for samples with Sc content up to 0.25 of the $P6_3cm$ to $P6_3/mmc$ transition happens above the measured temperature of 1200 °C. The transition temperature gradually decreases with

scandium content from 1150 °C for compounds with $x = 0.50$, to around 800 °C for $x = 0.75$. Particle morphology analysis indicated the drastic decrease of average particle size from ~2.726 μm without doping down to ~0.962 μm at 0.75 of Sc doping. However, the largest changes were observed when the scandium content was near the phase transition boundary, and was even observed to have increased up to ~1.669 μm when the x value reached 1.00. The particle morphology was more of a semi-spherical shape for compounds with dominant orthorhombic and cubic structures and in the case of hexagonal structure, the particles more resembled sharp rectangular shapes. The local iron ion environment and its oxidation state remained relatively stable in all compounds under study as confirmed by the XPS data. The analysis of magnetic properties revealed several important changes. Firstly, for samples with dominant hexagonal structure ($0.25 \leq x \leq 0.75$) the spin reorientation transition temperature T_N gradually increased from 156 K to 170 K, furthermore a potential glass transition temperature T_f was also observed in the same samples. An abrupt increase in remnant magnetization was also observed below the temperature of around ~160 K. However, this increase was much less pronounced in samples with higher Sc content. The temperature dependent magnetization data confirm the presence of non-zero remanent magnetization at temperatures above the mentioned spin reorientation temperature (T_N).

Acknowledgements

This project has received funding from the European Union's Horizon 2020 research and innovation programme under the Marie Skłodowska-Curie grant agreement No 778070 – TransFerr – H2020-MSCA-RISE-2017. G.N. gratefully acknowledges the Center of

573 Spectroscopic Characterization of Materials and Electronic/Molecular Processes
574 (SPECTROVERSUM Infrastructure) for use of Raman spectrometer.

575

576 **References**

577 [1] A. Pakalniskis, A. Marsalka, R. Raudonis, V. Balevicius, A. Zarkov, R. Skaudzius, A.
578 Kareiva, Sol-gel synthesis and study of praseodymium substitution effects in yttrium
579 aluminium garnet $Y_{3-x}Pr_xAl_5O_{12}$, Opt. Mater. (Amst). 111 (n.d.) 110586.
580 https://doi.org/10.1016/j.optmat.2020.110586.

581 [2] D. V. Karpinsky, O.M. Fesenko, M. V. Silibin, S. V. Dubkov, M. Chaika, A.
582 Yaremkevich, A. Lukowiak, Y. Gerasymchuk, W. Stręk, A. Pakalniškis, R. Skaudzius, A.
583 Kareiva, Y.M. Fomichov, V. V. Shvartsman, S. V. Kalinin, N. V. Morozovsky, A.N.
584 Morozovska, Ferromagnetic-like behavior of $Bi_{0.9}La_{0.1}FeO_3$–KBr nanocomposites, Sci.
585 Rep. 9 (2019). https://doi.org/10.1038/s41598-019-46834-0.

586 [3] A. Pakalniškis, R. Skaudžius, D. V. Zhaludkevich, A.L. Zhaludkevich, D.O. Alikin, A.S.
587 Abramov, T. Murauskas, V.Y. Shur, A.A. Dronov, M. V. Silibin, A. Selskis, R.
588 Ramanauskas, A. Lukowiak, W. Strek, D. V. Karpinsky, A. Kareiva, Morphotropic phase
589 boundary in Sm-substituted $BiFeO_3$ ceramics: Local vs microscopic approaches, J. Alloys
590 Compd. 875 (2021) 159994. https://doi.org/10.1016/j.jallcom.2021.159994.

591 [4] G. Inkrataite, A. Zabiliute-Karaliune, J. Aglinskaite, P. Vitta, K. Kristinaityte, A.
592 Marsalka, R. Skaudzius, Study of YAG : Ce and Polymer Composite Properties for
593 Application in LED Devices, Chempluschem. 85 (2020) 1504–1510.
594 https://doi.org/10.1002/cplu.202000318.

595 [5] T. Rojac, A. Bencan, B. Malic, G. Tutuncu, J.L. Jones, J.E. Daniels, D. Damjanovic,
596 $BiFeO_3$ Ceramics: Processing, Electrical, and Electromechanical Properties, J. Am.
597 Ceram. Soc. 97 (2014) 1993–2011. https://doi.org/10.1111/jace.12982.

598 [6] F. Shojaei, W.-J. Yin, Stability Trend of Tilted Perovskites, J. Phys. Chem. C. 122 (2018)
599 15214–15219. https://doi.org/10.1021/acs.jpcc.8b04875.

600 [7] E.A.R. Assirey, Perovskite synthesis, properties and their related biochemical and
601 industrial application, Saudi Pharm. J. 27 (2019) 817–829.
602 https://doi.org/10.1016/j.jsps.2019.05.003.

603 [8] M.A. Peña, J.L.G. Fierro, Chemical structures and performance of perovskite oxides,
604 Chem. Rev. 101 (2001) 1981–2017. https://doi.org/10.1021/cr980129f.

605 [9] H. Liu, X. Yang, A brief review on perovskite multiferroics, Ferroelectrics. 507 (2017).
606 https://doi.org/10.1080/00150193.2017.1283171.

607 [10] K. Wang, C. Han, Z. Shao, J. Qiu, S. Wang, S. Liu, K. Wang, C. Han, Z.P. Shao, S.M.
608 Liu, J.S. Qiu, S.B. Wang, Perovskite Oxide Catalysts for Advanced Oxidation Reactions,
609 Adv. Funct. Mater. 31 (2021) 2102089. https://doi.org/10.1002/ADFM.202102089.

[11] W. Eerenstein, N.D. Mathur, J.F. Scott, Multiferroic and magnetoelectric materials, Nature. 442 (2006) 759–765. https://doi.org/10.1038/nature05023.

[12] S.W. Cheong, M. Mostovoy, Multiferroics: a magnetic twist for ferroelectricity, Nat. Mater. 2007 61. 6 (2007) 13–20. https://doi.org/10.1038/nmat1804.

[13] I.H. Lone, J. Aslam, N.R.E.E. Radwan, A.H. Bashal, A.F.A.A. Ajlouni, A. Akhter, Multiferroic ABO_3 Transition Metal Oxides: a Rare Interaction of Ferroelectricity and Magnetism, Nanoscale Res. Lett. 14 (2019) 142. https://doi.org/10.1186/s11671-019-2961-7.

[14] N.A. Spaldin, R. Ramesh, Advances in magnetoelectric multiferroics, Nat. Mater. 18 (2019) 203–212. https://doi.org/10.1038/s41563-018-0275-2.

[15] N.A. Hill, Why Are There so Few Magnetic Ferroelectrics?, J. Phys. Chem. B. 104 (2000) 6694–6709. https://doi.org/10.1021/jp000114x.

[16] B.B. Van Aken, T.T.M. Palstra, A. Filippetti, N.A. Spaldin, The origin of ferroelectricity in magnetoelectric $YMnO_3$, Nat. Mater. 2004 33. 3 (2004) 164–170. https://doi.org/10.1038/nmat1080.

[17] M. Eibschütz, H.J. Guggenheim, S.H. Wemple, I. Camlibel, M. DiDomenico, Ferroelectricity in $BaM^{2+}F_4$, Phys. Lett. A. 29 (1969) 409–410. https://doi.org/10.1016/0375-9601(69)90332-6.

[18] M. Fiebig, T. Lottermoser, D. Meier, M. Trassin, The evolution of multiferroics, Nat. Rev. Mater. 1 (2016) 1–14. https://doi.org/10.1038/natrevmats.2016.46.

[19] U. Chowdhury, S. Goswami, A. Roy, S. Rajput, A.K. Mall, R. Gupta, S.D. Kaushik, V. Siruguri, S. Saravanakumar, S. Israel, R. Saravanan, A. Senyshyn, T. Chatterji, J.F. Scott, A. Garg, D. Bhattacharya, Origin of ferroelectricity in orthorhombic $LuFeO_3$, Phys. Rev. B. 100 (2019) 195116. https://doi.org/10.1103/PhysRevB.100.195116.

[20] T. Kimura, T. Goto, H. Shintani, K. Ishizaka, T. Arima, Y. Tokura, Magnetic control of ferroelectric polarization, Nature. 426 (2003) 55–58. https://doi.org/10.1038/nature02018.

[21] R. Ramesh, N.A. Spaldin, Multiferroics: progress and prospects in thin films, Nat. Mater. 2007 61. 6 (2007) 21–29. https://doi.org/10.1038/nmat1805.

[22] S.M. Disseler, J.A. Borchers, C.M. Brooks, J.A. Mundy, J.A. Moyer, D.A. Hillsberry, E.L. Thies, D.A. Tenne, J. Heron, M.E. Holtz, J.D. Clarkson, G.M. Stiehl, P. Schiffer, D.A. Muller, D.G. Schlom, W.D. Ratcliff, Magnetic Structure and Ordering of Multiferroic Hexagonal $LuFeO_3$, Phys. Rev. Lett. 114 (2015) 217602. https://doi.org/10.1103/PhysRevLett.114.217602.

[23] D. Sando, A. Agbelele, C. Daumont, D. Rahmedov, W. Ren, I.C. Infante, S. Lisenkov, S. Prosandeev, S. Fusil, E. Jacquet, C. Carrétéro, S. Petit, M. Cazayous, J. Juraszek, J.M. Le Breton, L. Bellaiche, B. Dkhil, A. Barthélémy, M. Bibes, Control of ferroelectricity and magnetism in multi-ferroic $BiFeO_3$ by epitaxial strain, Philos. Trans. R. Soc. A Math. Phys. Eng. Sci. 372 (2014). https://doi.org/10.1098/rsta.2012.0438.

[24] N.M.R. Alikhanov, M.K. Rabadanov, F.F. Orudzhev, S.K. Gadzhimagomedov, R.M.

649 Emirov, S.A. Sadykov, S.N. Kallaev, S.M. Ramazanov, K.G. Abdulvakhidov, D. Sobola,
650 Size-dependent structural parameters, optical, and magnetic properties of facile
651 synthesized pure-phase $BiFeO_3$, J. Mater. Sci. Mater. Electron. 32 (2021) 13323–13335.
652 https://doi.org/10.1007/s10854-021-05911-9.

653 [25] G. Catalan, J.F. Scott, Physics and Applications of Bismuth Ferrite, Adv. Mater. 21 (2009)
654 2463–2485. https://doi.org/10.1002/adma.200802849.

655 [26] M. Čebela, D. Zagorac, K. Batalović, J. Radaković, B. Stojadinović, V. Spasojević, R.
656 Hercigonja, $BiFeO_3$ perovskites: A multidisciplinary approach to multiferroics, Ceram.
657 Int. 43 (2017) 1256–1264. https://doi.org/10.1016/J.CERAMINT.2016.10.074.

658 [27] J. Liu, T.L. Sun, X.Q. Liu, H. Tian, T.T. Gao, X.M. Chen, A Novel Room-Temperature
659 Multiferroic System of Hexagonal $Lu_{1-x}In_xFeO_3$, Adv. Funct. Mater. 28 (2018) 1706062.
660 https://doi.org/10.1002/ADFM.201706062.

661 [28] M. Ye, D. Vanderbilt, Magnetic charges and magnetoelectricity in hexagonal rare-earth
662 manganites and ferrites, Phys. Rev. B. 92 (2015) 035107.
663 https://doi.org/10.1103/PhysRevB.92.035107.

664 [29] S. Leelashree, S.N. Kaul, S. Srinath, Effect of progressive substitution of Lu by Ho on the
665 structural and dielectric properties of nanocrystalline $LuFeO_3$ orthoferrite, Mater. Res.
666 Bull. 145 (2022) 111570. https://doi.org/10.1016/J.MATERRESBULL.2021.111570.

667 [30] L. Zhang, X.M. Chen, Dielectric relaxation in $LuFeO_3$ ceramics, Solid State Commun.
668 149 (2009) 1317–1321. https://doi.org/10.1016/J.SSC.2009.05.036.

669 [31] S.M. Disseler, X. Luo, B. Gao, Y.S. Oh, R. Hu, Y. Wang, D. Quintana, A. Zhang, Q.
670 Huang, J.W. Lau, R.L. Paul, J.W. Lynn, S.-W. Cheong, W.D. Ratcliff, Multiferroicity in
671 Doped Hexagonal $LuFeO_3$, Phys. Rev. B. 92 (2015) 054435–054435.
672 https://doi.org/10.1103/PhysRevB.92.054435.

673 [32] A.S. Gibbs, K.S. Knight, P. Lightfoot, High-temperature phase transitions of hexagonal
674 $YMnO_3$, Phys. Rev. B. 83 (2011) 094111. https://doi.org/10.1103/PhysRevB.83.094111.

675 [33] C.J. Howard, B.J. Campbell, H.T. Stokes, M.A. Carpenter, R.I. Thomson, Crystal and
676 magnetic structures of hexagonal $YMnO_3$, Acta Crystallogr. Sect. B Struct. Sci. Cryst.
677 Eng. Mater. 69 (2013) 534–540. https://doi.org/10.1107/S205251921302993X.

678 [34] J.A. Moyer, R. Misra, J.A. Mundy, C.M. Brooks, J.T. Heron, D.A. Muller, D.G. Schlom,
679 P. Schiffer, Intrinsic magnetic properties of hexagonal $LuFeO_3$ and the effects of
680 nonstoichiometry, APL Mater. 2 (2014) 012106. https://doi.org/10.1063/1.4861795.

681 [35] W. Wang, J. Zhao, W. Wang, Z. Gai, N. Balke, M. Chi, H.N. Lee, W. Tian, L. Zhu, X.
682 Cheng, D.J. Keavney, J. Yi, T.Z. Ward, P.C. Snijders, H.M. Christen, W. Wu, J. Shen, X.
683 Xu, Room-temperature multiferroic hexagonal $LuFeO_3$ films, Phys. Rev. Lett. 110 (2013).
684 https://doi.org/10.1103/PHYSREVLETT.110.237601.

685 [36] A. Masuno, S. Sakai, Y. Arai, H. Tomioka, F. Otsubo, H. Inoue, C. Moriyoshi, Y.
686 Kuroiwa, J. Yu, Structure and Physical Properties of Metastable Hexagonal $LuFeO_3$,
687 Ferroelectrics. 378 (2009) 169–174. https://doi.org/10.1080/00150190902848719.

[37] Y.K. Jeong, J.-H. Lee, S.-J. Ahn, H.M. Jang, Epitaxially Constrained Hexagonal Ferroelectricity and Canted Triangular Spin Order in $LuFeO_3$ Thin Films, Chem. Mater. 24 (2012) 2426–2428. https://doi.org/10.1021/cm300846j.

[38] O. Polat, M. Coskun, Y. Yildirim, P. Roupcova, D. Sobola, C. Sen, Z. Durmus, M. Caglar, A. Turut, Variation in the dielectric and magnetic characteristics of multiferroic $LuFeO_3$ as a result of cobalt substitution at Fe sites, J. Alloys Compd. 963 (2023) 170939. https://doi.org/10.1016/J.JALLCOM.2023.170939.

[39] J. White, K. Sinha, X. Xu, Structural phase diagram and magnetic properties of Sc-substituted rare earth ferrites $R_{1-x}Sc_xFeO_3$ (R = Lu, Yb, Er, and Ho), J. Appl. Phys. 125 (2019) 244101. https://doi.org/10.1063/1.5098488.

[40] K. Du, B. Gao, Y. Wang, X. Xu, J. Kim, R. Hu, F.-T. Huang, S.-W. Cheong, Vortex ferroelectric domains, large-loop weak ferromagnetic domains, and their decoupling in hexagonal (Lu, Sc)FeO_3, Npj. Quant. Mater. 3 (2018) 33. https://doi.org/10.1038/s41535-018-0106-3.

[41] S. Deng, J. Li, D.R. Småbråten, S. Shen, W. Wang, J. Zhao, J. Tao, U. Aschauer, J. Chen, Y. Zhu, J. Zhu, Critical Role of Sc Substitution in Modulating Ferroelectricity in Multiferroic $LuFeO_3$, Nano Lett. 21 (2021) 6648–6655. https://doi.org/10.1021/ACS.NANOLETT.1C02123.

[42] S. Sadhukhan, A. Mitra, A.S. Mahapatra, P.K. Chakrabarti, Room temperature multiferroicity of hexagonal $LuFeO_3$ and its enhancement by co-doping in $Lu_{0.9}Co_{0.1}Fe_{0.9}Ti_{0.1}O_3$ nanoparticle system, J. Alloys Compd. 956 (2023) 170351. https://doi.org/10.1016/J.JALLCOM.2023.170351.

[43] M. Li, H. Tan, W. Duan, Hexagonal rare-earth manganites and ferrites: a review of improper ferroelectricity, magnetoelectric coupling, and unusual domain walls, Phys. Chem. Chem. Phys. 22 (2020) 14415–14432. https://doi.org/10.1039/D0CP02195D.

[44] Y.S. Tang, S.M. Wang, L. Lin, V. Ovidiu Garlea, T. Zou, S.H. Zheng, H.-M. Zhang, J.T. Zhou, Z.L. Luo, Z.B. Yan, S. Dong, T. Charlton, J.-M. Liu, Magnetic structure and multiferroicity of Sc-substituted hexagonal $YbFeO_3$, Phys. Rev. B. 103 (2021) 174102. https://doi.org/10.1103/PhysRevB.103.174102.

[45] J. Rodríguez-Carvajal, Recent advances in magnetic structure determination by neutron powder diffraction, Phys. B. Condens. Matter. 192 (1993) 55–69. https://doi.org/10.1016/0921-4526(93)90108-I.

[46] J. Schindelin, I. Arganda-Carreras, E. Frise, V. Kaynig, M. Longair, T. Pietzsch, S. Preibisch, C. Rueden, S. Saalfeld, B. Schmid, J.Y. Tinevez, D.J. White, V. Hartenstein, K. Eliceiri, P. Tomancak, A. Cardona, Fiji: An open-source platform for biological-image analysis, Nat. Methods. 9 (2012) 676–682. https://doi.org/10.1038/nmeth.2019.

[47] A.S. Bhalla, R. Guo, R. Roy, The perovskite structure—a review of its role in ceramic science and technology, Mater. Res. Innov. 4 (2000) 3–26. https://doi.org/10.1007/s100190000062.

[48] E. Magome, C. Moriyoshi, Y. Kuroiwa, A. Masuno, H. Inoue, Noncentrosymmetric

Structure of $LuFeO_3$ in Metastable State, Jpn. J. Appl. Phys. 49 (2010) 09ME06. https://doi.org/10.1143/JJAP.49.09ME06.

[49] S. Chaturvedi, S.K. Singh, P. Shyam, M.M. Shirolkar, S. Krishna, R. Boomishankar, S. Ogale, Nanoscale $LuFeO_3$: shape dependent ortho/hexa-phase constitution and nanogenerator application, Nanoscale. 10 (2018) 21406–21413. https://doi.org/10.1039/C8NR07825D.

[50] T. Katayama, Y. Hamasaki, S. Yasui, A. Miyahara, M. Itoh, Epitaxial thin film growth of garnet-, $GdFeO_3$-, and $YMnO_3$-type $LuFeO_3$ using pulsed laser deposition, Thin Solid Films. 642 (2017) 41–44. https://doi.org/10.1016/J.TSF.2017.09.013.

[51] A.S. Ryabova, S.Y. Istomin, K.A. Dosaev, A. Bonnefont, J. Hadermann, N.A. Arkharova, A.S. Orekhov, R.P. Sena, V.A. Saveleva, G. Kéranguéven, E. V. Antipov, E.R. Savinova, G.A. Tsirlina, Mn_2O_3 oxide with bixbyite structure for the electrochemical oxygen reduction reaction in alkaline media: Highly active if properly manipulated, Electrochim. Acta. 367 (2021) 137378. https://doi.org/10.1016/J.ELECTACTA.2020.137378.

[52] T. Kawamoto, K. Fujita, I. Yamada, T. Matoba, S.J. Kim, P. Gao, X. Pan, S.D. Findlay, C. Tassel, H. Kageyama, A.J. Studer, J. Hester, T. Irifune, H. Akamatsu, K. Tanaka, Room-Temperature Polar Ferromagnet $ScFeO_3$ Transformed from a High-Pressure Orthorhombic Perovskite Phase, J. Am. Chem. Soc. 136 (2014) 15291–15299. https://doi.org/10.1021/ja507958z.

[53] A. Pakalniškis, D.O. Alikin, A.P. Turygin, A.L. Zhaludkevich, M. V. Silibin, D. V. Zhaludkevich, G. Niaura, A. Zarkov, R. Skaudžius, D. V. Karpinsky, A. Kareiva, Crystal Structure and Concentration-Driven Phase Transitions in $Lu_{(1-x)}Sc_xFeO_3$ ($0 \leq x \leq 1$) Prepared by the Sol–Gel Method, Materials (Basel). 15 (2022) 1048. https://doi.org/10.3390/ma15031048.

[54] S. Leelashree, S. Srinath, Investigation of Structural, Ferroelectric, and Magnetic Properties of La-Doped $LuFeO_3$ Nanoparticles, J. Supercond. Nov. Magn. 33 (2020) 1587–1591. https://doi.org/10.1007/s10948-019-5114-4.

[55] M. V. Abrashev, N.D. Todorov, J. Geshev, Raman spectra of R_2O_3 (R—rare earth) sesquioxides with C-type bixbyite crystal structure: A comparative study, J. Appl. Phys. 116 (2014) 103508. https://doi.org/10.1063/1.4894775.

[56] S. Venugopalan, M.M. Becker, Raman scattering study of $LuFeO_3$, J. Chem. Phys. 93 (1990) 3833–3836. https://doi.org/10.1063/1.458768.

[57] A. Pakalniškis, A. Lukowiak, G. Niaura, P. Głuchowski, D.V. Karpinsky, D.O. Alikin, A.S. Abramov, A. Zhaludkevich, M. Silibin, A.L. Kholkin, R. Skaudžius, W. Strek, A. Kareiva, Nanoscale ferroelectricity in pseudo-cubic sol-gel derived barium titanate - bismuth ferrite ($BaTiO_3$– $BiFeO_3$) solid solutions, J. Alloys Compd. (2020) 154632. https://doi.org/10.1016/j.jallcom.2020.154632.

[58] D. Karoblis, A. Zarkov, K. Mazeika, D. Baltrunas, G. Niaura, A. Beganskiene, A. Kareiva, Sol-gel synthesis, structural, morphological and magnetic properties of $BaTiO_3$–$BiMnO_3$ solid solutions, Ceram. Int. 46 (2020) 16459–16464. https://doi.org/10.1016/j.ceramint.2020.03.209.

[59] L. Martín-Carrón, A. De Andrés, M.J. Martínez-Lope, M.T. Casais, J.A. Alonso, Raman phonons as a probe of disorder, fluctuations, and local structure in doped and undoped orthorhombic and rhombohedral manganites, Phys. Rev. B. 66 (2002) 174303. https://doi.org/10.1103/PhysRevB.66.174303.

[60] J. Andreasson, J. Holmlund, R. Rauer, M. Käll, L. Börjesson, C.S. Knee, A.K. Eriksson, S.G. Eriksson, M. Rübhausen, R.P. Chaudhury, Electron-phonon interactions in perovskites containing Fe and Cr studied by Raman scattering using oxygen-isotope and cation substitution, Phys. Rev. B - Condens. Matter Mater. Phys. 78 (2008) 235103. https://doi.org/10.1103/PhysRevB.78.235103.

[61] D.V. V. Karpinsky, A. Pakalniškis, G. Niaura, D.V. V. Zhaludkevich, A.L.L. Zhaludkevich, S.I.I. Latushka, M. Silibin, M. Serdechnova, V.M.M. Garamus, A. Lukowiak, W. Stręk, M. Kaya, R. Skaudžius, A. Kareiva, Evolution of the crystal structure and magnetic properties of Sm-doped $BiFeO_3$ ceramics across the phase boundary region, Ceram. Int. (2020). https://doi.org/10.1016/j.ceramint.2020.10.120.

[62] J. Ibáñez, O. Blázquez, S. Hernández, B. Garrido, P. Rodríguez-Hernández, A. Muñoz, M. Velázquez, P. Veber, F.J. Manjón, Lattice dynamics study of cubic Tb_2O_3, J. Raman Spectrosc. 49 (2018) 2021–2027. https://doi.org/10.1002/JRS.5488.

[63] D. Karoblis, A. Zarkov, K. Mazeika, D. Baltrunas, G. Niaura, A. Beganskiene, A. Kareiva, $YFeO_3$-$GdFeO_3$ solid solutions: Sol-gel synthesis, structural and magnetic properties, Solid State Sci. 118 (2021) 106632. https://doi.org/10.1016/J.SOLIDSTATESCIENCES.2021.106632.

[64] G. Inkrataite, M. Kemere, A. Sarakovskis, R. Skaudzius, Influence of boron on the essential properties for new generation scintillators, J. Alloys Compd. 875 (2021) 160002. https://doi.org/10.1016/j.jallcom.2021.160002.

[65] K.S. Kantharaj, G.V.J. Gowda, A. El-Denglawey, N. Ramprasad, A.T. Kozakov, A. V. Nikolsky, S. Kubrin, A. Gowda, V.J. Angadi, B.M. Raafat, M. Dongol, Study of the electronic structure of $LuFeO_3$ and $Lu(YFe)O_3$ nanoparticles by X-ray photoelectron spectroscopy and Mossbauer spectra, J. Mater. Sci. Mater. Electron. 33 (2022) 14178–14187. https://doi.org/10.1007/s10854-022-08347-x.

[66] H. Wei, Y. Yu, P. Feng, J. Xue, J. Pan, F. Zhao, Q. Wang, Controllable synthesis of $ScFeO_3$ ceramics with microstructural evolution for thin and broadband high-performance microwave absorption, J. Alloys Compd. 925 (2022) 166826. https://doi.org/10.1016/J.JALLCOM.2022.166826.

[67] M. Descostes, F. Mercier, N. Thromat, C. Beaucaire, M. Gautier-Soyer, Use of XPS in the determination of chemical environment and oxidation state of iron and sulfur samples: constitution of a data basis in binding energies for Fe and S reference compounds and applications to the evidence of surface species of an oxidized py, Appl. Surf. Sci. 165 (2000) 288–302. https://doi.org/10.1016/S0169-4332(00)00443-8.

[68] A.P. Grosvenor, B.A. Kobe, M.C. Biesinger, N.S. McIntyre, Investigation of multiplet splitting of Fe 2p XPS spectra and bonding in iron compounds, Surf. Interface Anal. 36 (2004) 1564–1574. https://doi.org/10.1002/sia.1984.

[69] R.P. Gupta, S.K. Sen, Calculation of multiplet structure of core p-vacancy levels. II, Phys. Rev. B. 12 (1975) 15. https://doi.org/10.1103/PhysRevB.12.15.

[70] R.P. Gupta, S.K. Sen, Calculation of multiplet structure of core p- vacancy levels, Phys. Rev. B. 10 (1974) 71–77. https://doi.org/10.1103/PhysRevB.10.71.

[71] N.S. McIntyre, D.G. Zetaruk, X-ray photoelectron spectroscopic studies of iron oxides, Anal. Chem. 49 (1977) 1521–1529. https://doi.org/10.1021/ac50019a016.

[72] O. Polat, The role of Os substitution on structural, magnetic, and optical features of LuFeO3, Solid State Sci. 132 (2022) 106981. https://doi.org/10.1016/j.solidstatesciences.2022.106981.

[73] W. Zhu, L. Pi, S. Tan, Y. Zhang, Anisotropy and extremely high coercivity in weak ferromagnetic $LuFeO_3$, Appl. Phys. Lett. 100 (2012) 52407. https://doi.org/10.1063/1.3681789/126876.

[74] Y. Brard, H. Fjellvg, B. Hauback, Investigation of bixbyite type scandium oxides involving a magnetic cation: $Sc_{2-x}Fe_xO_3$ ($0 \leq x \leq 1$), Solid State Commun. 151 (2011) 223–226. https://doi.org/10.1016/J.SSC.2010.11.028.

[75] P. Suresh, K. Vijaya Laxmi, A.K. Bera, S.M. Yusuf, B.L. Chittari, J. Jung, P.S. Anil Kumar, Magnetic ground state of the multiferroic hexagonal $LuFeO_3$, Phys. Rev. B. 97 (2018) 184419. https://doi.org/10.1103/PhysRevB.97.184419.

[76] L. Lin, H.M. Zhang, M.F. Liu, S. Shen, S. Zhou, D. Li, X. Wang, Z.B. Yan, Z.D. Zhang, J. Zhao, S. Dong, J.-M. Liu, Hexagonal phase stabilization and magnetic orders of multiferroic $Lu_{1-x}Sc_xFeO_3$, Phys. Rev. B. 93 (2016) 075146. https://doi.org/10.1103/PhysRevB.93.075146.

[77] H. Das, A.L. Wysocki, Y. Geng, W. Wu, C.J. Fennie, Bulk magnetoelectricity in the hexagonal manganites and ferrites, Nat. Commun. 5 (2014) 2998. https://doi.org/10.1038/ncomms3998.